ORCA – Online Research @ Cardiff

1   # Hydro-epidemiological modelling of bacterial transport and

2   # decay in nearshore coastal waters

3   Jonathan King[1,2], Reza Ahmadian[1,*], and Roger A. Falconer[1]

4   [1] Hydro-environmental Research Centre (HRC), School of Engineering, Cardiff

5   University, Cardiff, CF24 3AA, UK

6   [2] JBA Consulting, 1 Broughton Park, Old Lane North, Broughton, Skipton, North

7   Yorkshire, BD23 3FD

8   * Corresponding author. E-mail address: AhmadianR@cardiff.ac.uk (R. Ahmadian)

9   ## Abstract

10   In recent years, society has become more aware and concerned with the environmental and

11   human health impacts of population growth and urbanisation. In response, a number of

12   legislative measures have been introduced within Europe (and globally), which have sparked

13   much cross-disciplinary research aimed at predicting and quantifying these impacts, and

14   suggesting mitigation measures.

15   In response to such measures this paper is focused on improving current understanding of, and

16   simulating water quality, in the form of bacterial transport and decay, in the aquatic environment

17   and particularly in macro-tidal environments. A number of 2D and 3D hydro-epidemiological

18   models were developed using the TELEMAC suite to predict faecal bacterial levels for a data rich

19   pilot site, namely Swansea Bay, located in the south west of the UK, where more than 7,000 FIO

20   samples were taken and analysed over a two year period.

21   A comparison of 2D and 3D modelling approaches highlights the importance of accurately

22   representing source momentum terms in hydro-epidemiological models. Improvements in 2D

23   model bacterial concentration predictions were achieved by the application of a novel method for

representing beach sources within the nearshore zone of a macro-tidal environment. In addition, the use of a depth-varying decay rate was found to enhance the prediction of Faecal Indicator Organism concentrations in 3D models. Recommendations are made for the use of these novel approaches in future modelling studies.

1   Introduction

The health of nearshore coastal waters is a topic of great concern globally. As a result of population growth and industrialisation, the number of polluted discharges into water bodies has increased during the 20th and 21st centuries, with much detriment to the aquatic environment. Such contamination has far reaching consequences, which include: human health impacts through recreational activity (Weiskerger and Phanikumar, 2020) and the consumption of polluted food in the form of shellfish, reduced tourism, and economic losses (DeFlorio-Barker et al. 2018; Bussi et al. 2017; Given et al. 2006).

For example, domestic and international visitors to the coast contributed $6 billion to the UK economy in 2017 (BBC, 2017; Visit Britain, 2017). In a recent study, the Scottish Government (2018) predicted a loss of $3 million per year should bathing water quality not be maintained at an acceptable level at popular beaches. Another financial incentive is the healthcare savings associated with reduced exposure of beach goers to contaminated water (Given et al., 2006). For example, DeFlorio-Barker et al. (2018) estimated that recreational waterborne illnesses cost the US economy $2.2 to $3.7 billion every year. It is therefore important to address these issues by determining the primary sources of pollution at any one location, developing an understanding of the mechanisms which lead to adverse water quality, beach closure, and implementing mitigation strategies.

To ensure protecting human health as highlighted above, legislative measures have been introduced with regard to bathing water quality. The existing legislation applicable in the EU is the revised Bathing Waters Directive (rBWD) (European Parliament, 2006) which ensures the monitoring of water quality and defines acceptable standards, based on human health risk and following guidelines released by the World Health Organisation on safe standards for recreational waters (World Health Organization, 2003). The revised Bathing Waters Directive was introduced by the European Parliament in 2007 requiring Member States to ensure all bathing waters were of 'sufficient' quality by the close of the 2015 bathing season (European Parliament, 2006). Compliance criteria are based on the monitored concentration of two Faecal Indicator Organisms (FIOs); *Intestinal enterococci* and *Escherichia coli (E. coli)* in colony forming units per 100ml (cfu/100ml). The directive requires the concentration of these organisms to be monitored over consecutive bathing seasons (May to September), in accordance with a sampling calendar. Based on the Directive 2006/7/EC of the European Parliament, samples showing abnormally elevated concentrations, caused as a result of short-term pollution incidents, or contamination attributable to a cause, expected to last less than 72 hours, such as high level of pollution following a heavy rainfall may be disregarded and retaken (European Environment Agency, 2005). Efforts must also be made to reduce the risk of bather exposure to contaminants in addition to providing regular information on bathing water quality. Therefore, the directive requires the public to be made aware of short-term pollution incidences in advance, in order for these events to be disregarded, thereby making public health a key driver for prediction.

Due to the time lag between the collection and assessment of individual samples, monitoring in this manner is not a practical way of providing rapid public feedback to prevent exposure (Feng et al., 2015). To enable accurate and fast dissemination of information it is therefore in the interest of the governing authority to develop predictive tools to provide water quality forecasts and warning systems (Bedri et al., 2014, 2016; Chen and Liu, 2017; DHI, 2017a, b; Weiskerger and Phanikumar, 2020). Not only would this comply with the rBWD but it could enable the

78   identification, reduction and removal of major pollution sources, increasing the likelihood of a

79   bathing water being assigned Blue Flag status (Bedri et al., 2015; Lea, 1996).

80   There are two main approaches to the development of predictive tools to provide water quality

81   forecasts and warning systems: data driven modelling based on extensive field measurements,

82   and process-based hydro-epidemiological models. Herein the latter approach is used, with the aim

83   being to improve our understanding of fundamental processes affecting the fate and transport of

84   bacterial pollution, in order to enhance the management of bacterial sources, development of

85   predictive tools, and assessing beach monitoring and management practices.

86

87   This study examines and investigates the use of two novel techniques, as well as the methods

88   which have been used to date for the prediction of bacterial decay in 2D and 3D model frameworks,

89   using a data rich macro-tidal bay as a study site.

90

91   2   Methodology

92   2.1   Study Site

93   Swansea Bay is situated on the north shoreline of the Bristol Channel, located in the south west of

94   the UK, and is a popular location among tourists and the local community (see Figure 1). The Bay

95   contains two bathing water sites: Swansea Bay and Aberafan, both of which received a 'good'

96   rating in the most recent bathing water assessment period. Swansea Bay was chosen for this study

97   due to the tidal nature of the Bay, the number of FIO point sources and, more importantly, a large

98   quantity of measured FIO data, where more than 7,000 FIO samples were taken and analysed over

99   a two-year period.

100

101   The Bay is subject to 85 different inputs (see Figure 1b) including three main rivers discharging

102   into the Bay: The River Tawe, River Neath and River Afan. There is a semi submerged barrage

103   located on the River Tawe, which only overtops at tides over 3.05 m above Ordinance Datum.

104   However, the River Neath and River Afan are tidal up to about 10 km and 1 km upstream from

105   the coast, respectively. Primary surface water and sewage discharges were recorded at 15-

106   minute intervals over the 2011 bathing season (May - September) and October - November 2012

107   for the Smart Coasts project (Aberystwyth University and University College Dublin, 2018) as

108   shown in Figure 1c, although data were unavailable for Combined Sewer Overflow (CSO) spills.

109   The rBWD requires samples to be taken at a minimum depth of 0.5 m (Bedri et al., 2016;

110   Bomminayuni, 2015) at the Designated Sampling Point (DSP) for each bathing water site.

111   However, the tidal range in the Bay exceeds 10 m and the tidal flats are exposed up to a distance

112   of 1500 m from shore during high spring tides. This prevents readings being taken at each

113   bathing water site at only one location for the rBWD. Therefore, the water quality at Swansea

114   Bay and Aberafan were monitored along BW1 and BW2 transects respectively as shown in

115   Figure 1c. Figure 1c also depicts the locations of offshore sampling points used for model

116   validation and calibration. The variability in the sampling location is shown in Figure 2 which

117   presents the sampling points along BW1, recorded throughout the 2011 bathing season at 30-

118   minute intervals from 07:00 to 16:00.

119
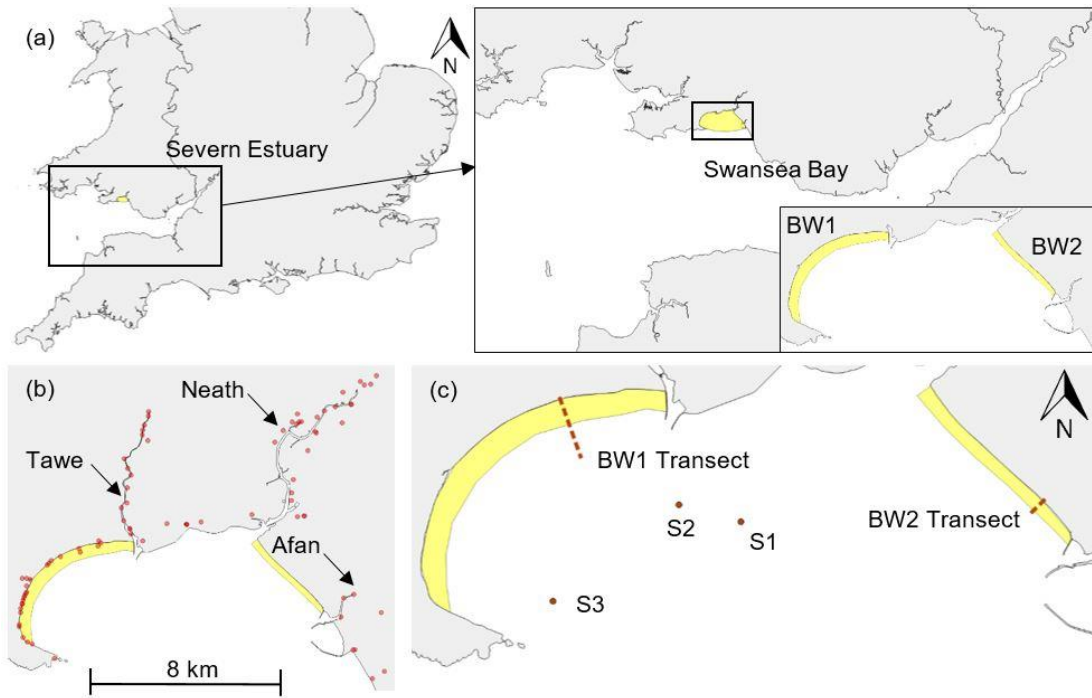
Figure 1: (a) Location of bathing waters within Swansea Bay, Severn Estuary, UK: BW1 - Swansea

Bay, BW2 – Aberafan (b) Location of FIO inputs (c) Location of transects (dashed lines) and

offshore monitoring points (dots)

123
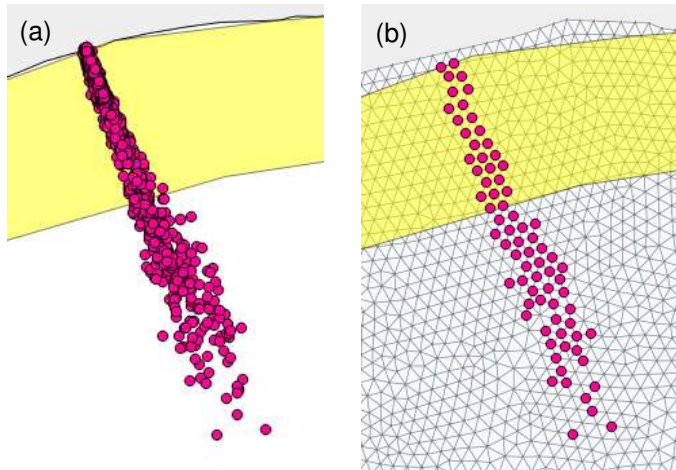
Figure 2: FIO sampling locations throughout the 2011 bathing season (a) [Aberystwyth University

and University College Dublin, 2018], and the respective 2D mesh nodes (b)

## 2.2   Hydrodynamic models

The open-source models TELEMAC-2D and TELEMAC-3D (Galland et al., 1991) were chosen for

this study to compliment previous research applications in the field of hydro-epidemiological

6

129   engineering (Abu Bakar et al., 2017a, Bedri et al., 2013; Kopmann and Markofsky, 2000).

130   Developed by Electricité de France, the models solve the Navier-Stokes Equations over an

131   unstructured finite element grid (Hervouet, 2007). Further details are provided in the next

132   section.

133

134   Two computational meshes of the Bristol Channel and Swansea Bay were created, one each for the

135   2D and 3D models. The 3D domain comprised a 2D mesh repeated over 5 uniformly distributed

136   sigma layers and extends over the same area apart from the rivers in Swansea Bay, as shown in

137   Figure 3. To remove the need for coupling with a 1D model, the 2D model was extended up the

138   River Tawe and to the tidal limits of the rivers Afan and Neath. However, these reaches were

139   excluded from the 3D model to reduce the computational time and unnecessary vertical

140   refinement in regions where 3D effects were of limited concern. Note that at the time of writing,

141   coupling between the latest release of TELEMAC-3D (v7p3r2), and the 1D river model TELEMAC-

142   MASCARET, was not possible.
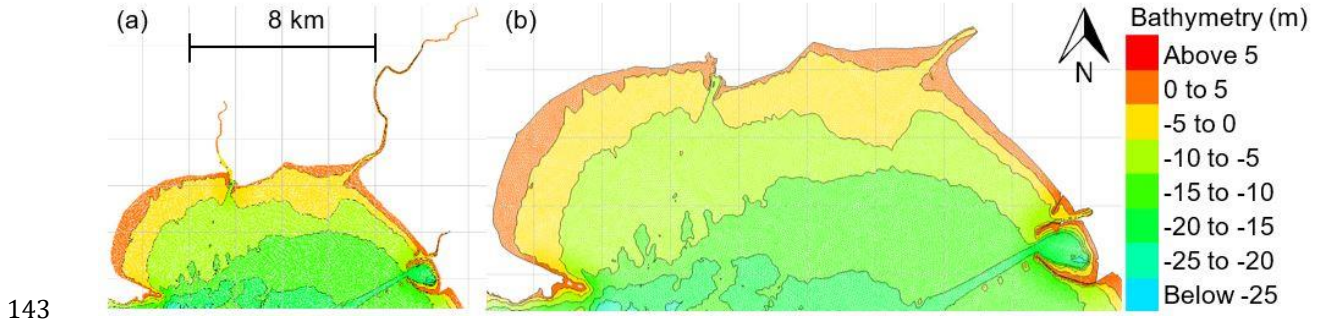
144   *Figure 3: Extent of 2D (a) and 3D (b) unstructured computational meshes of Swansea Bay.*

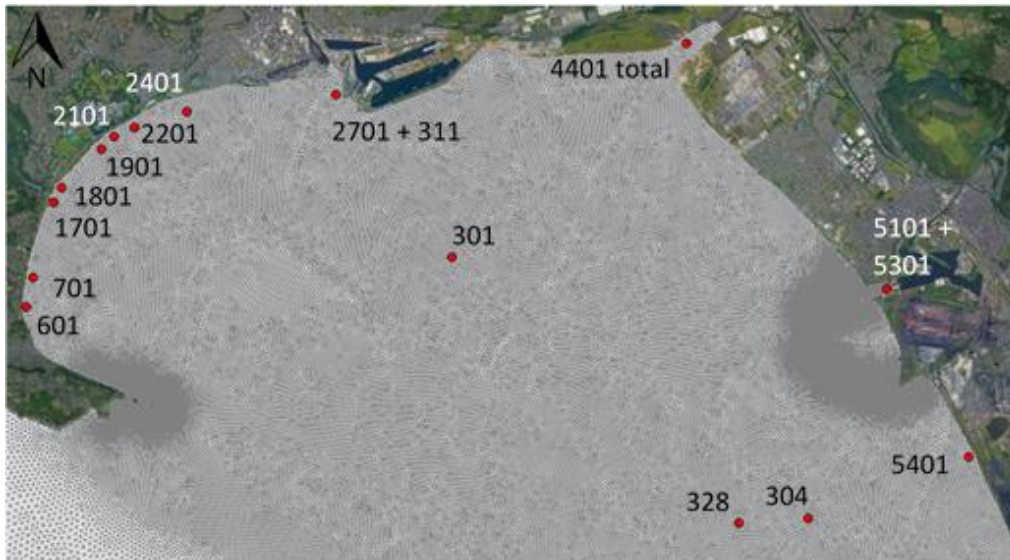145   *Bathymetry relative to mean sea level (MSL)*

146   Bacterial sources were included as a concentration (cfu/100 ml) time series. Source locations

147   within each domain are shown in Figures 4 and 5, respectively. In the 3D model, the bacterial

148   source inputs distributed within each reach were combined into a single source point, whereas

149   those in the 2D model retained their true position.

150
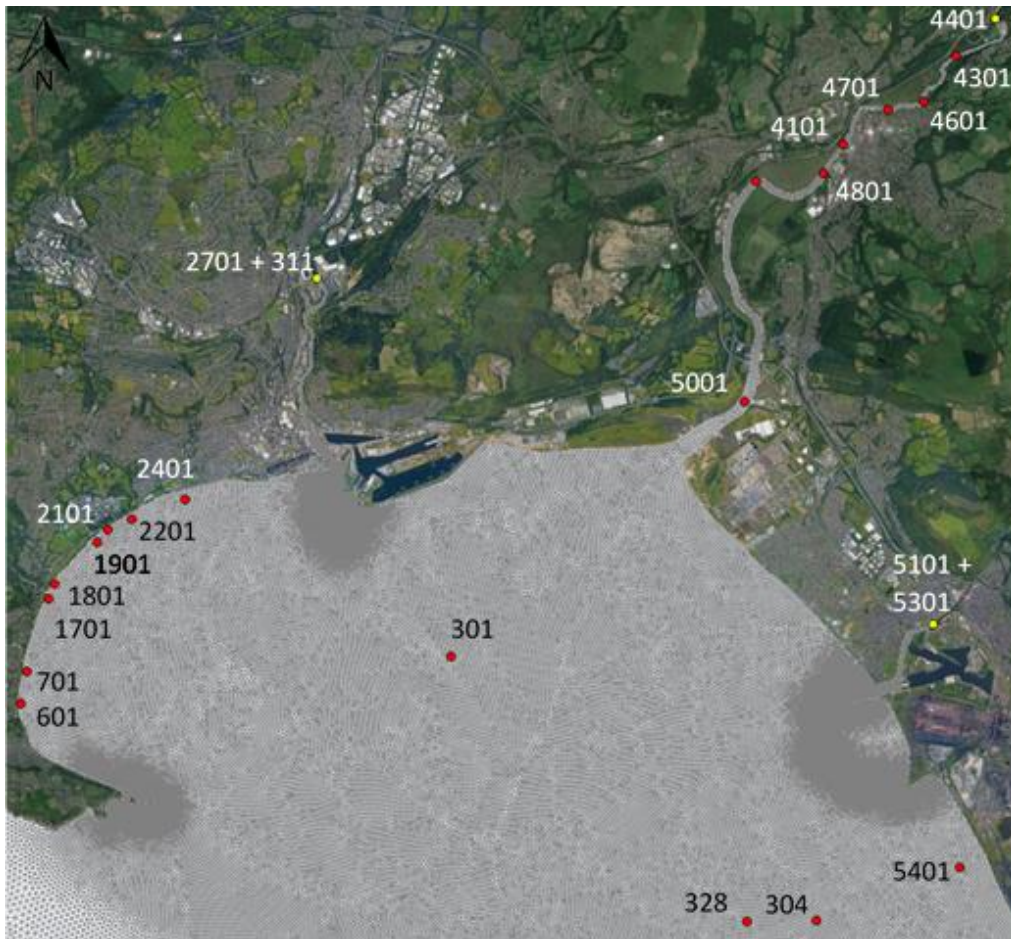
Figure 4: Primary input locations of bacterial sources within the 2D model domain of Swansea Bay

151

– year 2012; point sources (red dots) and boundary conditions (yellow dots) with the relative ID

152

No.

153

154

155

156

Both meshes extend from the River Severn tidal limit close to Gloucester to the outer Bristol

Channel close to Lundy Island, as shown in Figure 6, in order to capture the hydrodynamics of the

Severn Estuary and Bristol Channel as has been widely used in previous studies (Ahmadian et al,

2014, Coz et al., 2019 and Guo et al., 2020). Bathymetry data was obtained from EDINA Digimap,

relative to chart datum (CD), at a 30 m grid resolution (The University of Edinburgh, 2016a, b). An

open boundary with a tidal water level series is imposed along the westward edge of the domain

where the Bristol Channel meets the Celtic Sea.
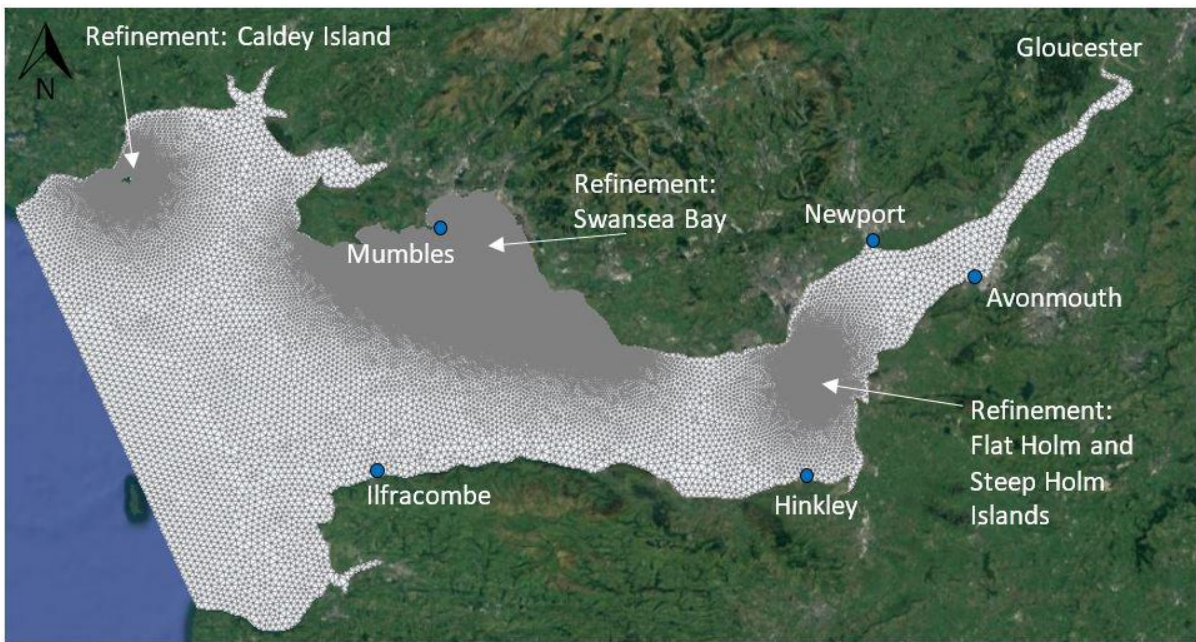
164

165

166 *Figure 6: Extent of the unstructured computational mesh within the Bristol Channel and Severn*

167 *Estuary, showing the water level monitoring locations (blue dots)*

168 Stapleton et al. (2007a) found that a coarse grid (600 m by 600 m), was incapable of capturing

169 localised features, such as pollutant plume shapes. The minimum grid size in the bay was limited

170 to 30 m to capture bathymetric features as closely as possible. Therefore, the mesh size in Swansea

171 Bay was determined based on sensitivity analysis of the different meshes. Two computational

172 meshes were developed; using a 25 m and 50 m mesh in Swansea Bay, and increasing at a uniform

173 rate of 1.2 to 1,000 m in the outer Bristol Channel and the Severn Estuary. From the grid

174 dependence model tests the model results were found to be insensitive to the mesh size for the

175 grid resolutions studies and a 50 m grid size was therefore used within Swansea Bay to increase

176 computational efficiency. Further refinements of the grid size to 10m were used at various

177 locations within the Bay to capture shoreline complexities. The 2D mesh contained 142,533 nodes

178 and 281,440 elements, the 3D mesh contained 133,341 nodes and 264,237 elements, repeated

179 over 5 sigma layers giving 666,705 nodes and 1,059,648 elements in total. As for similar studies

180 the Smagorinski turbulence closure model was used in the horizontal (Bedri et al., 2015, 2013,

181 Abu Bakar et al., 2017b, Guo et al., 2020) and vertical directions.

2.3 Fate and transport of bacteria: governing equations

Bacteria was simulated in TELEMAC as a non-conservative passive numerical tracer, represented by the advection-diffusion equation. Herein this is referred to as the tracer equation, written in 3D as shown in Equation 1 (Hervouet, 2007):

$$\frac{\partial C}{\partial t} + U\frac{\partial C}{\partial x} + V\frac{\partial C}{\partial y} + W\frac{\partial C}{\partial z} = \frac{\partial}{\partial x}\left(v_T\frac{\partial C}{\partial x}\right) + \frac{\partial}{\partial y}\left(v_T\frac{\partial C}{\partial y}\right) + \frac{\partial}{\partial z}\left(v_T\frac{\partial C}{\partial z}\right) + S_C \qquad \textit{1}$$

where C is the tracer concentration (units depend on the tracer but for bacteria it is cfu/100ml), t is time (s), h is the water depth (m), U, V and W are layer averaged velocities (m/s) in the x, y and z directions respectively, v_T is the diffusion coefficient (m/s^2). S_C is the source or sink term, including both explicit and implicit terms. Bacterial decay is governed by the first order decay rate k which is commonly written as shown in Equation 2 (Chapra, 1997; Thomann and Mueller, 1987).

$$\frac{\partial C}{\partial t} = -kC \qquad \textit{2}$$

The decay rate k (1/d) is transposed into a T$_{90}$ value, i.e. the time required for the concentration to reduce by 90% (Guillaud et al., 1997), as shown in Equation 3. This is traditionally required as a user input value in TELEMAC and many other models.

$$T90 = \frac{2.303}{k} \qquad \textit{3}$$

202 Multiple methods exist to determine the T_{90} value, and which have been applied in a number of

203 studies (Chapra, 1997; Droste, 1997; Mancini, 1978; Stapleton et al., 2007a; Ahmadian et al., 2010;

204 de Brauwere et al., 2011; Bedri et al., 2013; Boye et al., 2015; Huang et al., 2015; Abu Bakar et al.,

205 2017b). Two methods have been implemented in this paper: a pre-defined constant decay rate,

206 and that proposed by Stapeleton et al (2007a). The widely used approach proposed by Mancini

207 (1978) was also used within the study but is not described herein due to its exclusion of sediment

208 effects and the inclusion of non-site-specific data. For further information, see King (2019).

209

210 Stapleton et al. (2007a) carried out a study on water samples taken from the Bristol Channel and

211 Severn Estuary to determine the impact of light intensity and turbidity on bacterial decay. As a

212 result of laboratory experiments, the T_{90} decay rate for Enterococci was found to follow Equations

213 4 to 8:

214

$$T_{90} = T_{90_2} + \left(T_{90_1} - T_{90_{*1}}\right) \qquad 4$$

215

$$T_{90_1} = \frac{ln10}{K_B * 60 * I} \qquad 5$$

216

$$T_{90_{*1}} = \frac{ln10}{K_B * 60 * I^{exp}} \qquad 6$$

217

$$LogT_{90_2} = (0.0047 * Turbidity) + 0.677 \qquad 7$$

218

$$Turbidity = 139.479 * Log(SS) - 244.736 \pm 32.678 \qquad 8$$

219

220

221 where I is the sunlight intensity (W/m^2), I^{exp} is the fixed irradiance for the experiments (26,014

222 W/m^2), T_{90*1} is the sunlight dependent Enterococci mortality rate, T_{901} is the *Enterococci* mortality

223 rate obtained from laboratory experiments, T_{902} is the turbidity related *Enterococci* mortality rate

224 and $K_B = 1.1 \times 10^{-5}$ and SS is the suspended sediment concentration (mg/l). While Stapleton et al.

225 (2007a) only investigated the decay of *Enterococci*, the value for *E. coli* can be calculated using an

226 appropriate magnitude of K_B ($K_B = 1.3 \times 10^{-5}$) (Alkan et al. 1995).

227

2.4   Model refinements

2.4.1   Depth-varying decay rate

230 Bedri et al. (2013) published the first attempt at including a spatially and temporally variant decay

231 rate within TELEMAC-3D, using the decay formula proposed by Mancini (1978), but neglected the

232 ability of a 3D model to incorporate light attenuation throughout the water column. The decay rate

233 was calculated using Equations 9 and 10 (Bedri et al., 2013):

234

$$k_i = \alpha \bar{I} \qquad\qquad 9$$

235

$$\bar{I} = \frac{I_a}{k_e H}\left(1 - e^{-k_e H}\right) \qquad\qquad 10$$

236

237

238 where H is the water depth (m), I_α is the average daily light intensity (langleys/h), $\bar{I}$ is the depth

239 averaged light intensity, αs a proportionality constant and k_e is the light attenuation coefficient

240 (1/m). Equation 10 is an integration of the Beer-Lambert law which, over the fully mixed water

241 depth (Xu et al., 2002; Chapra, 1997), can be expressed as:

242

$$I(z) = I_0 e^{-k_e H} \qquad\qquad 11$$

243

244 where I_0 is the surface light intensity. The light attenuation coefficient k_e (1/m) may be calculated

245 using (Chapra, 1997):

246

$$k_e = 0.55\, SS \qquad\qquad 12$$

247

248 where SS is the suspended solids concentration (mg/l). For a finite element model, such as

249 TELEMAC, the governing equations are solved at each node and Equation 11 can be used without

250 integration, such that the irradiance induced decay rate at depth is given by Equation 13 (Chapra,

251 1997):

252

$$k_i(z) = \alpha I(z) \qquad\qquad 13$$

253

254 where the light penetration at depth is given as a function of z, i.e. $I(z)$, and where this function is

255 calculated using the Beer-Lambert law (see Equation 11). Experimental studies have confirmed

256 this reduction in the decay rate at increasing depths below the water surface (Mattioli et al., 2017).

257 For completeness and to assist future studies a comparison is made with the application of

258 Equation 11 in a finite volume model: the average light penetrating over each layer would be used.

259 This can be calculated using the layer averaged Beer-Lambert law and using the mean value

260 theorem for integrals:

261

$$\bar{I}_{layer} = \frac{\alpha I_0}{k_e\left(z_{bottom} - z_{top}\right)}\left(e^{-k_e z_{top}} - e^{-k_e z_{bottom}}\right) \qquad\qquad 14$$

262

263   where z_{bottom} and z_{top}, are the elevations at the bottom and top of the horizontal layer respectively.

264   Figure 7 presents depth-irradiance curves calculated using Equations 10, 11 and 14. Equations 11

265   and 14 exhibit a comparable reduction in light intensity with depth, whereas the rate of reduction

266   is less when using Equation 10 (i.e. a depth averaged representation). Since TELEMAC is a finite

267   element model, Equation 11 was used in this study.
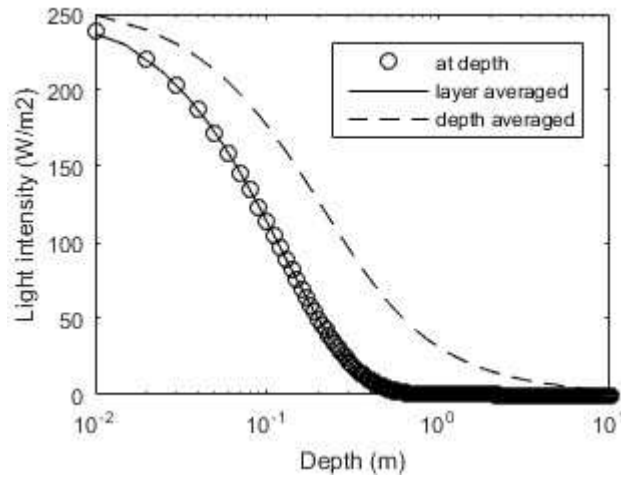
268

269   *Figure 7: Comparison between irradiance at depth, calculated using: Equations 10 (depth*

270   *averaged), 11 (at depth), 14 (layer averaged) and k_e calculated using Equation 12 where SS =*

271   *84.82 mg/l*

272   **2.4.2   Representation of beach sources**

273   In modelling studies to date, bacterial sources such as CSOs and outfalls have been represented at

274   a single point source within numerical models. However, when the grid size is too coarse, a source

275   is distributed over a disproportionately large area and the local bathymetric features, such as that

276   shown in Figure 8, are not captured accurately.

277   Furthermore, in models such as TELEMAC, where the minimum permissible water depth is 0 m,

278   when these sources are released within shallow gradient regions the contaminated water spreads

279   over a large area in a thin film, as shown in Figure 9 (i.e. of depth less than 1 cm, up to 1×10^{-5} m).

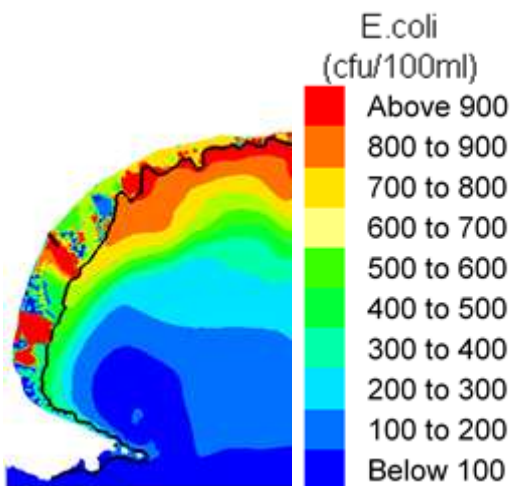280   For further details see King (2019).

281

15

282

283

284

285 *Figure 8: Stream track of beach source, South Wales, UK*


286

287 *Figure 9: Depth averaged E.coli concentration in Swansea Bay at mid-tide; black line indicates a*

288 *depth of 0.05m (i.e. the waterline)*

289 While inaccurate, this is necessary to ensure mass conservation. In reality, these inputs form small

290 streams in the beach sand (as illustrated in Figure 8), which run from the source point to the tide

291 line. These streams can run for up to a kilometre, from the sea defence wall to the tide line, at low

292 spring tide for this case study site. The major streams at Swansea Bay were tracked by staff at

293 Natural Resources Wales and Swansea City Council for this research study and as a part of Smart

294   Coast project (Aberystwyth University and University College Dublin, 2018). The path of these

295   streams can be seen in Figure 10.
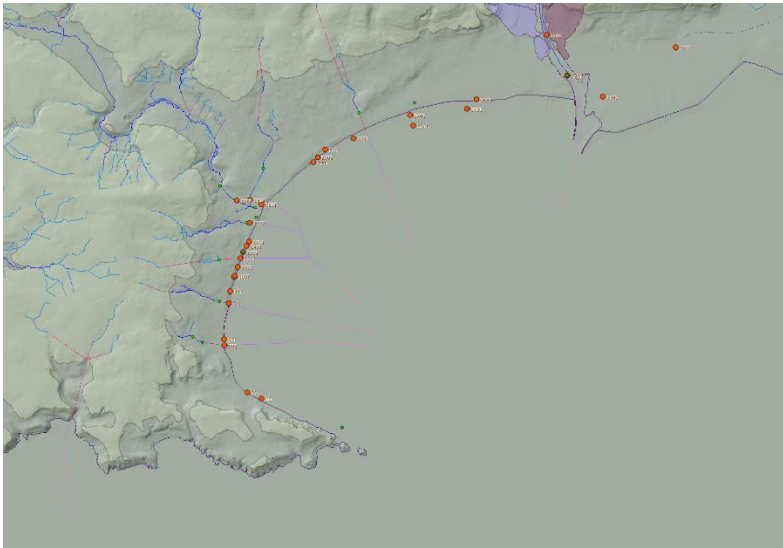
296

297   *Figure 10: Stream tracks of beach sources along Swansea Bay; purple lines and red dots respectively*

298   *(Aberystwyth University and University College Dublin, 2018)*

299   From Figure 10 it is clear that including sources at high water will not represent what happens in

300   the field and will cause inaccuracy in the predictions. The method proposed herein implements a

301   mobile source point which tracks the waterfront along the stream path and activates releases

302   based on the depth field. To achieve this, each source point is treated as a transect running from

303   the sea wall to the low water line based on the field tracking of that stream. Each transect is

304   represented by multiple source points, which discharge the same volume of water and

305   concentration of bacteria. The source release location is changeable to ensure release is always at

306   a point below the water line, mimicking transport within a stream. To ensure mass conservation,

307   modifications to the TELEMAC source code only permit one point to discharge per time step, i.e.

308   that which is closest to, and below, the waterline. Figure 11 shows the multiple source points

309   which were used along the transects for Swansea Bay. Up to 10 source points were selected on

310   each transect in this study as can be seen in the figure. However, more source points can be

311   considered if the path of the streams are more complicated.
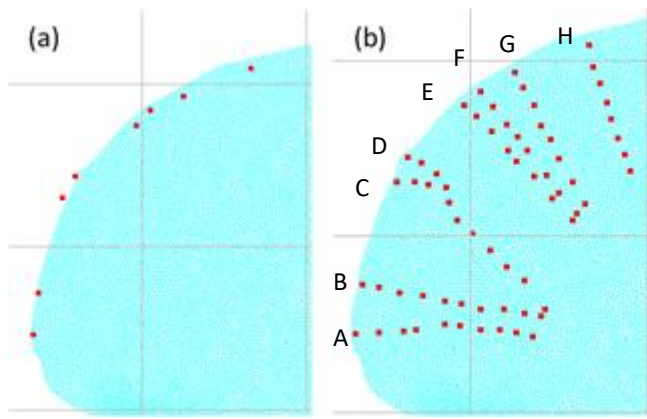
Figure 11: Static source points at the outlet location and respective source transects along Swansea Bay beach; (a) and (b) respectively

An illustration of this source representation for release at four different tidal phases is shown in Figure 12a to d. It can be seen as the tide recedes the 0.05 m depth threshold is activated at different source points along the transect (black dot). The source points along each transect were processed by multiple CPUs in parallel and the code was modified to implement this. Further information on the implementation of this method when using parallel computing methods can be found in King (2019). A similar approach was used by Feng et al. (2015), who developed a microbial transport model accounting for loading from beach sand and storm water run-off at a beach in Florida, U.S. However, the model was reduced to a 1D case for a single lumped source, and solved using the finite difference method. The grid followed a transect perpendicular to the straight uniform shoreline, which was assumed to be representative of the beach.
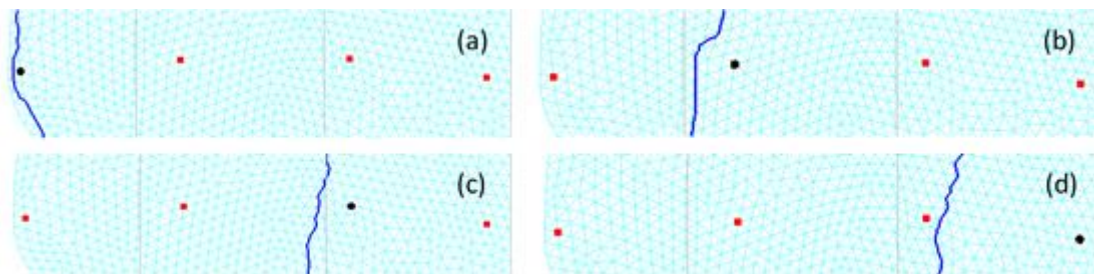

Figure 12: Illustration of improved source representation at four different tidal phases for transect A in Figure 11; blue line = threshold depth (0.05 m) which retreats seaward (right) from figure a to d, red squares = transect points, black circle

18

330

2.4.3   Parameter selection

332   Swansea Bay is well mixed (Ahmadian et al., 2013) with variations in temperature and salinity

333   being shown in Figure 13. As variations through the water column are negligible they were not

334   considered herein. Typically, in such environments a 2D modelling approach would be adopted,

335   thus making it an ideal environment to study the difference between using depth-averaged and

336   depth-varying approaches to calculate bacterial decay due to light intensity. Water temperature

337   and salinity were set at 15℃ and 32 ppt respectively to match values used in previous studies

338   (Aberystwyth University and University College Dublin, 2018; White et al., 2014).
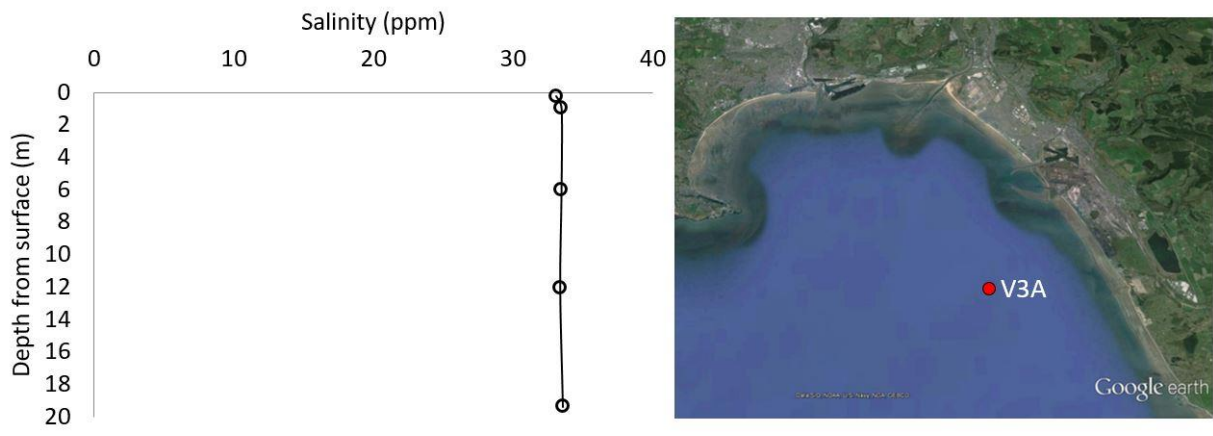
339

340   *Figure 13: Typical vertical salinity profile in Swansea Bay (location V3A; Ahmadian et al., 2013)*

341   The interaction between suspended sediment levels and FIOs has been studied previously and its

342   importance highlighted (Haung et al., 2015 and 2018, Ahmadian et al., 2010, Yang et al., 2008).

343   Since this study was mainly focused on implementation of the decay rate in the absence of

344   sediment data, sediment modelling was not considered as a part of this study. While surveys have

345   shown variations in suspended sediment concentrations throughout the water column, data are

346   sparse and a constant value of 84.82mg/l was assumed, based on measurements taken nearby at

347   Langland Bay and Porthcawl (Stapleton et al., 2007b). Based on this assumption Equations 4 to 8

348   are considered a function of light intensity and water depth. The relationship between the T_{90}

349   value and these variables is shown in Figure 14, using Latin hypercube sensitivity analysis (Iman,

350   2008; Stein, 1987). The water depth, which varied up to the maximum natural (i.e. not dredged)

351   water depth in Swansea Bay and irradiance varied over the feasible parameter range from the

352   reviewed literature (Stapleton et al., 2007a) and site measurements (Aberystwyth University and

353   University College Dublin, 2018).

354
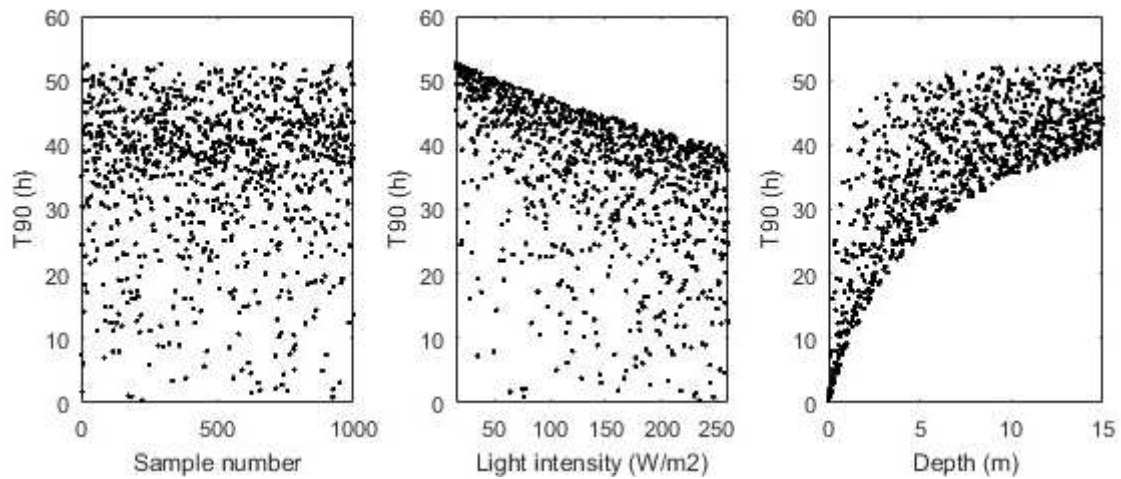
Figure 14: Latin hypercube sensitivity analysis of decay rate based on depth and irradiance

variations with suspended solid concentrations, salinity and temperature being considered

constant

358   Data recorded over the 2012 simulation period shows an average daily maximum of 170 W/m^2.

359   This fits within the 0 to 260 W/m^2 range of light intensity reported by Stapleton et al. (2007a). A

360   sine function, covering the range 0 to pi, was used to represent the variation in light intensity over

361   daylight hours (06:00 to 18:00), as proposed by Boye et al. (2015) and as shown in Figure 15.

362   Night-time values were recorded at 0.15 W/m^2. However, a lower limit of 15 W/m^2 was placed on

363   this value to prevent the T_{90} value tending towards infinity as depth and solar intensity

364   approached zero.

365
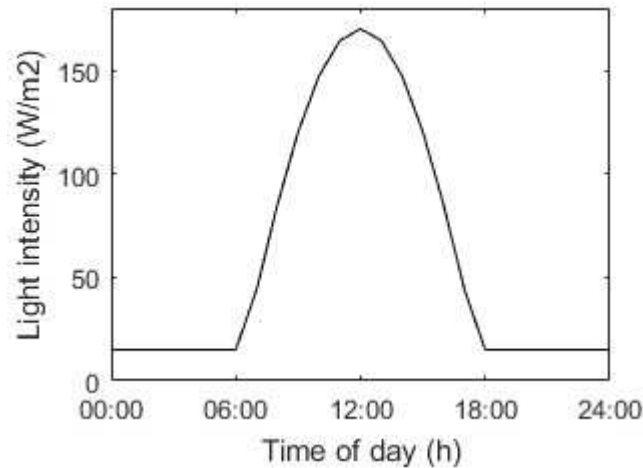
Figure 15: Assumed light intensity function over a typical day

3   Hydrodynamic model validation

A constant Manning's coefficient was used throughout the model domain. Based on the range of suggested roughness values presented in Chow (1959), water levels were calibrated by testing values of 0.02, 0.025 and 0.03 respectively, which were deemed suitable for excavated or dredged channels, and clean, straight main channels. The model was found to have low sensitivity to the bed roughness and a value of 0.025 was selected as that producing the best fit. Calibration and validation of water levels were initially carried out against tide gauge records provided by the British Oceanographic Data Centre (BODC) (https://www.bodc.ac.uk/), at four sites throughout the domain, as shown in Figure 6, over a spring-neap tidal cycle. Two sites, namely Illfracombe and Avonmouth, were used for model calibration and the sites at Mumbles and Hinkley Point were used for model validation. A plot comparing measured and predicted water levels at the Mumbles site, which is located at the Western edge of Swansea Bay, is shown in Figure 16. The Root Mean Square Error (RMSE) and Nash Sutcliffe Efficiency (NSE) (Nash and Sutcliffe, 1970; Coz et al., 2019) values were used to assess the correlation of the predicted and measured data. The RMSE and NSE values for the Mumbles site were 0.31 and 0.99, respectively, which showed good correlation between the measured and predicted data. There is a gap in the BODC data record for this site, which can be seen in Figure 16.

21

384

385   Further validation of water level predictions was carried out using Acoustic Doppler Current

386   Profilers (ADCP), deployed at 5 sites within Swansea Bay (as shown in Figure 17), from

387   21/07/2012 to 28/08/2012 (Aberystwyth University and University College Dublin, 2018; EMU

388   Limited, 2012) . The survey was carried out using a bed mounted Nortek Aquapro (EMU Limited,

389   2012). This further validation also confirmed good correlation between the measured and

390   predicted water levels. The velocity magnitudes and directions predicted by the model were

391   validated against the ADCP measurements, which were averaged over depth. The comparisons of

392   the measured and predicted velocity magnitudes and directions showed that model predictions

393   matched the measured data and that the model predictions were reliable. Typical comparisons of

394   measured and predicted velocity magnitudes and directions are shown in Figures 15 and 16.

395   Current direction are presented with respect to due north.
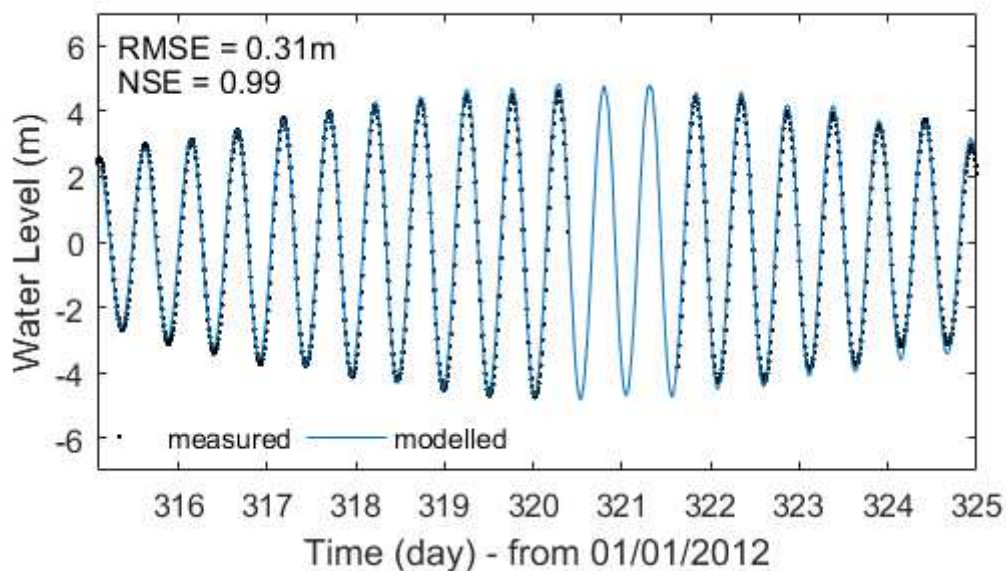
396

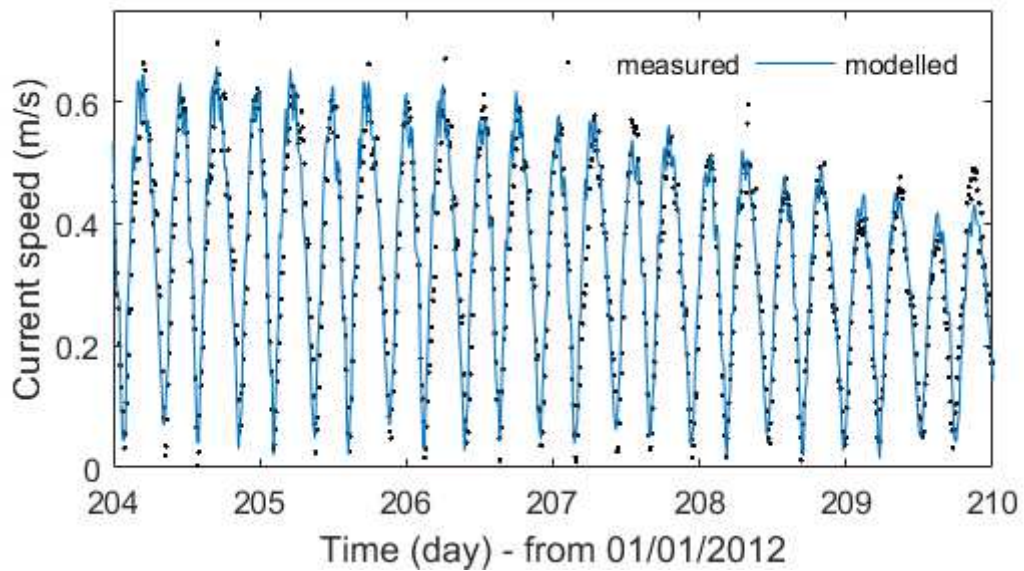397   *Figure 16: Plot of calibrated water levels measured at Mumbles, adjusted relative to MSL, n = 0.025*

398
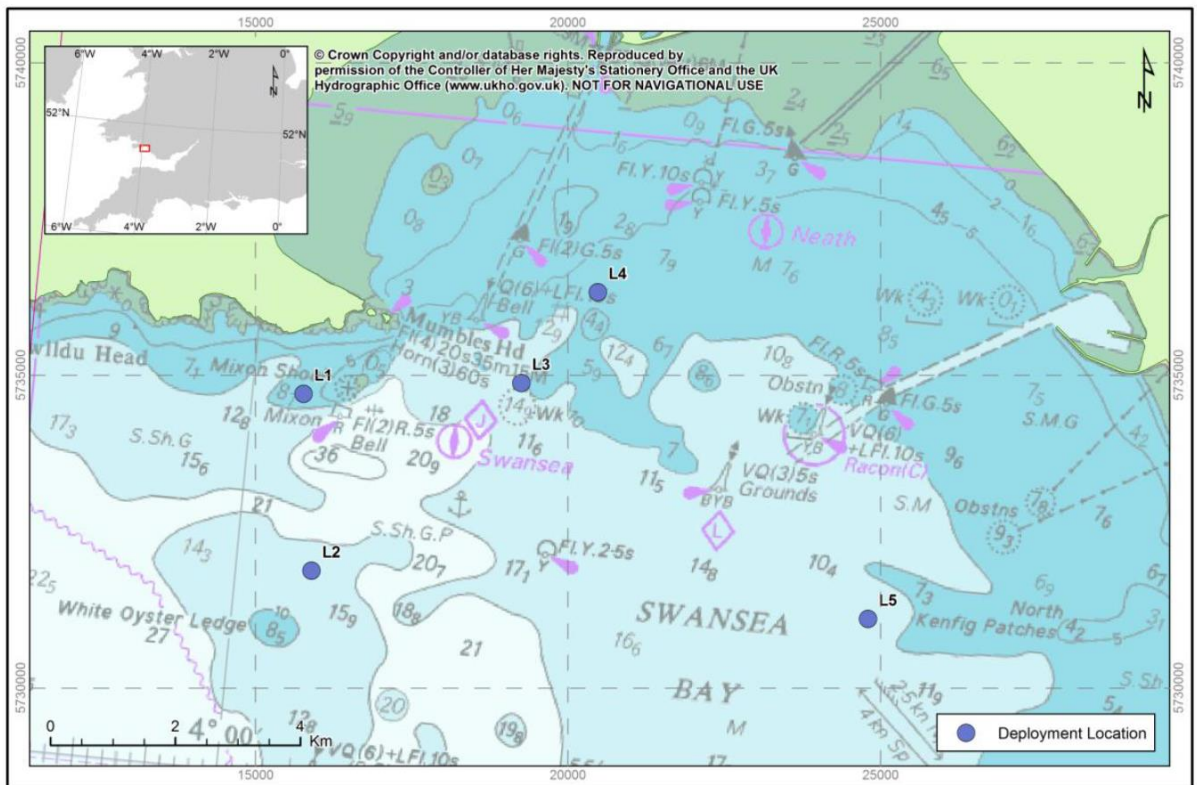
399
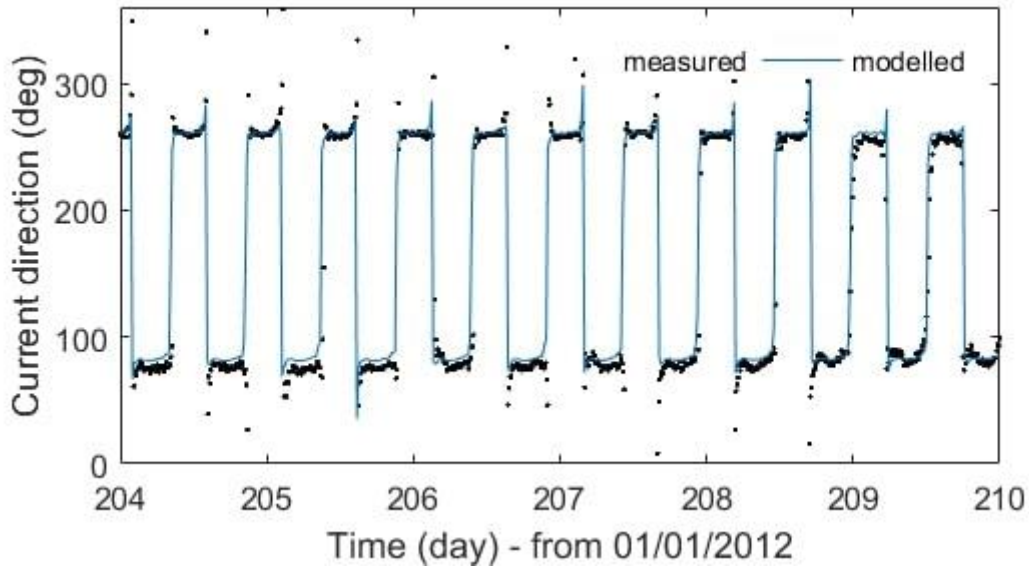
Figure 17: ADCP survey locations in Swansea Bay

401

Figure 18: Plot of validated current speed in Swansea Bay at location L2

403

Figure 19: Plot of validated current direction in Swansea Bay at location L2

404

4   Results

405

406   The model performance was next assessed using the *E. coli* records taken on 15th November 2012

407   (Aberystwyth University and University College Dublin, 2018). Monitoring at the Swansea Bay and

408   Aberafan DSPs was done along the transects shown in Figure 1. The measured and predicted

409   values were compared using the new developments discussed in 2.4.1 and 2.4.2, to assess the

410   performance of each method. For supplementary data omitted from this paper for brevity, see

411   King (2019).

412

413   Figure 20 presents a comparison between the 2D and 3D modelled *E. coli* concentration

414   predictions at the Swansea Bay DSP, using stationary point sources and a depth-averaged decay

415   function. To mirror the sampling strategy used in the field the predictions shown are taken at the

416   shallowest transect point greater than or equal to the sampling depth (0.5 m, see Section 2.1 and

417   Figure 2b). Thus, the line plots shown correspond to multiple locations. Note that all 3D results

418   presented herein have been averaged over the vertical layers to provide an indication of the

419   concentration throughout the water column, rather than within a single layer. It can be seen in

420   Figure 20 that the 2D model predicts higher concentrations than the 3D model.

421

422 The predicted concentrations using the depth averaged decay function at all points along the DSP

423 transect within the 2D model are plotted in Figure 21, while the concentration plots around the

424 DSP and the monitoring points along the DSP transect are shown in Figure 22. It can be seen in

425 Figure 21 that at any point in time, there are significant spatial differences in the predicted *E. coli*

426 concentrations at each transect point, with a range of up to half the magnitude of the highest

427 predicted concentrations. The point which is considered a best fit to the measured data has been

428 highlighted.

429

430 Figure 23 presents a comparison between the measured and predicted *E.coli* concentrations at the

431 Swansea Bay DSP using depth-averaged and varying decay rates. It can be seen that lower

432 concentrations were predicted when using the depth-varying decay function.
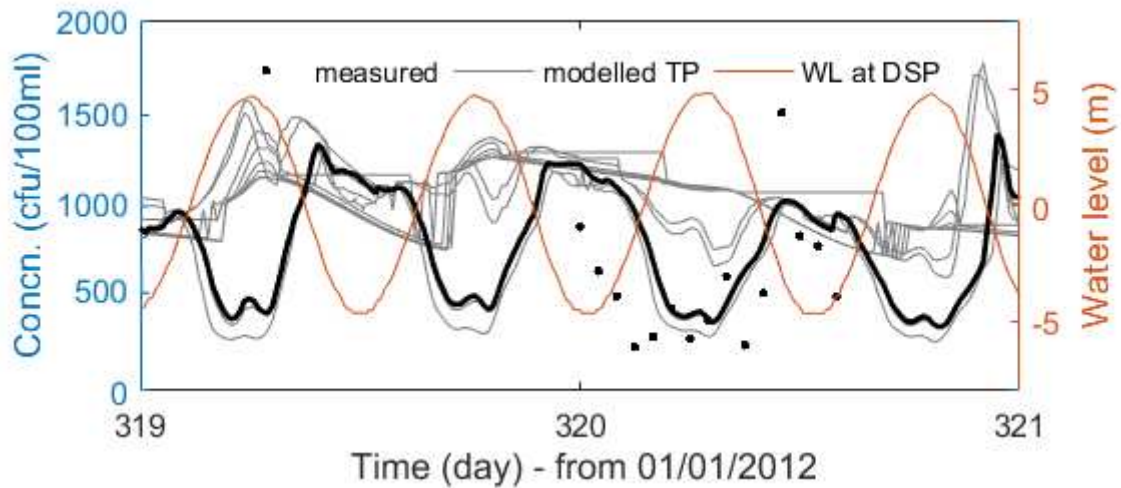
433

434
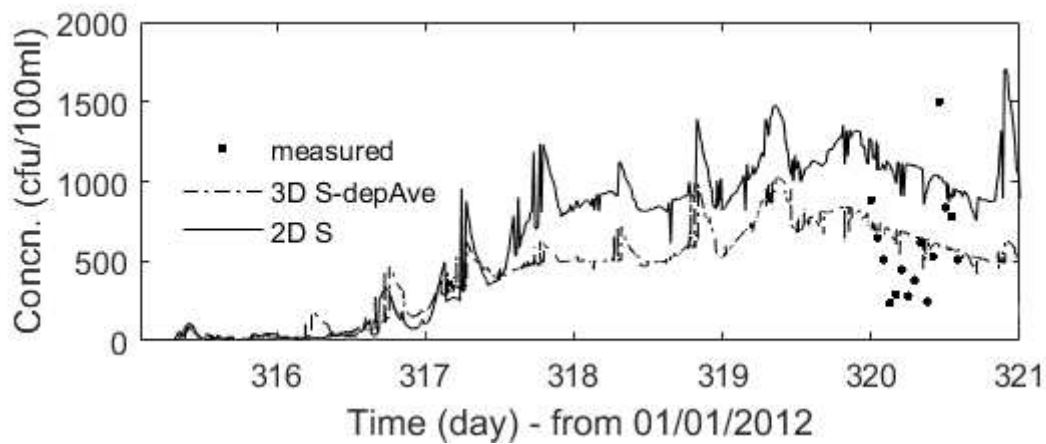
435

436 *Figure 20: Comparison between the measured and predicted E.coli concentrations at the Swansea*

437 *Bay DSP, using the Stapleton et al. (2007a) (S) decay function in the 2D and 3D models*

438

439   *Figure 21: Comparison between the measured and predicted E. coli concentrations at each*

440   *monitoring location along the Swansea Bay DSP transect (TP), using the Stapleton et al. (2007a)*

441   *decay function in the 2D model. Plotted alongside the predicted water level at the most offshore*

442   *monitoring location*

443

444   *Figure 22: Surface plot of the predicted E. coli concentrations along the Swansea Bay DSP transects,*

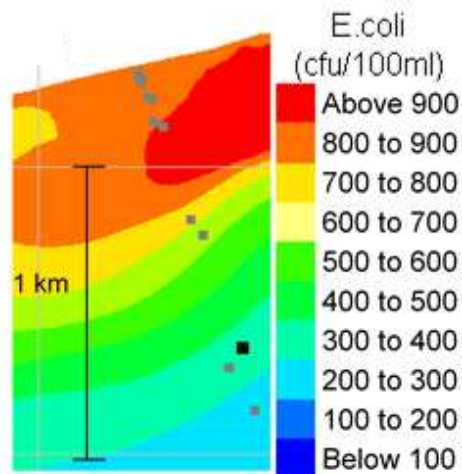445   *using the Stapleton et al. (2007a) decay function in the 2D model at 19:11:57 on 15/11/12 (high*

446   *tide)*
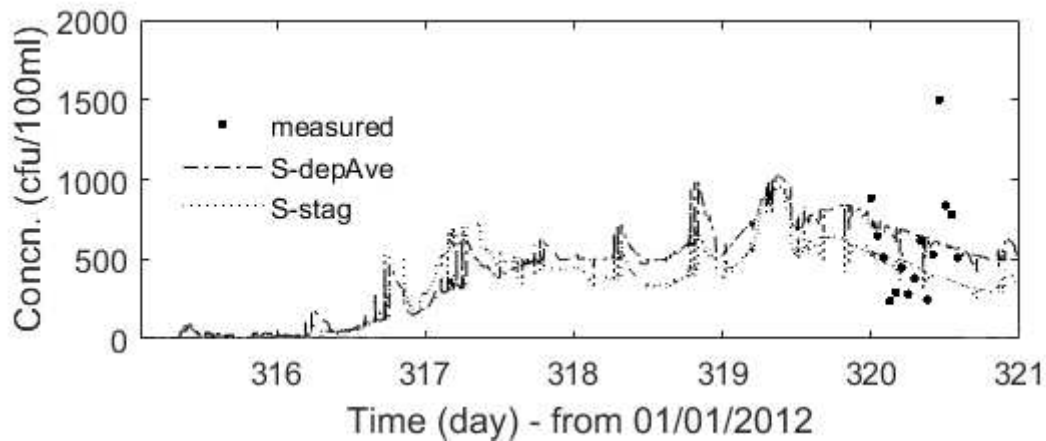
447

448 *Figure 23: Comparison between the measured and predicted E.coli concentrations at the Swansea*

449 *Bay DSP using depth-averaged and varying Stapleton et al. (2007a) (S) decay functions in the 3D*

450 *model*

451 Plots comparing the measured and predicted *E.coli* concentrations at the Swansea Bay DSP using

452 the static and improved source release models are shown in Figures 24 and 25. Figure 24 presents

453 this comparison at the Swansea Bay DSP whereas Figure 25 includes the wider Bay area and

454 highlights the spatial variability in concentration predictions between the methods.
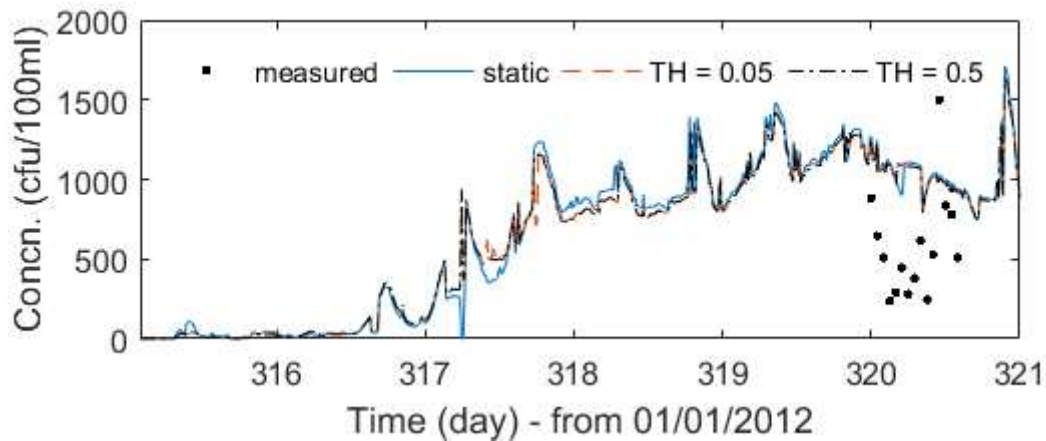
455

456 *Figure 24: Comparison between the predicted E. coli concentrations at the Swansea Bay DSP, using*

457 *static sources, and improved source representation with two threshold depths (TH)*

458
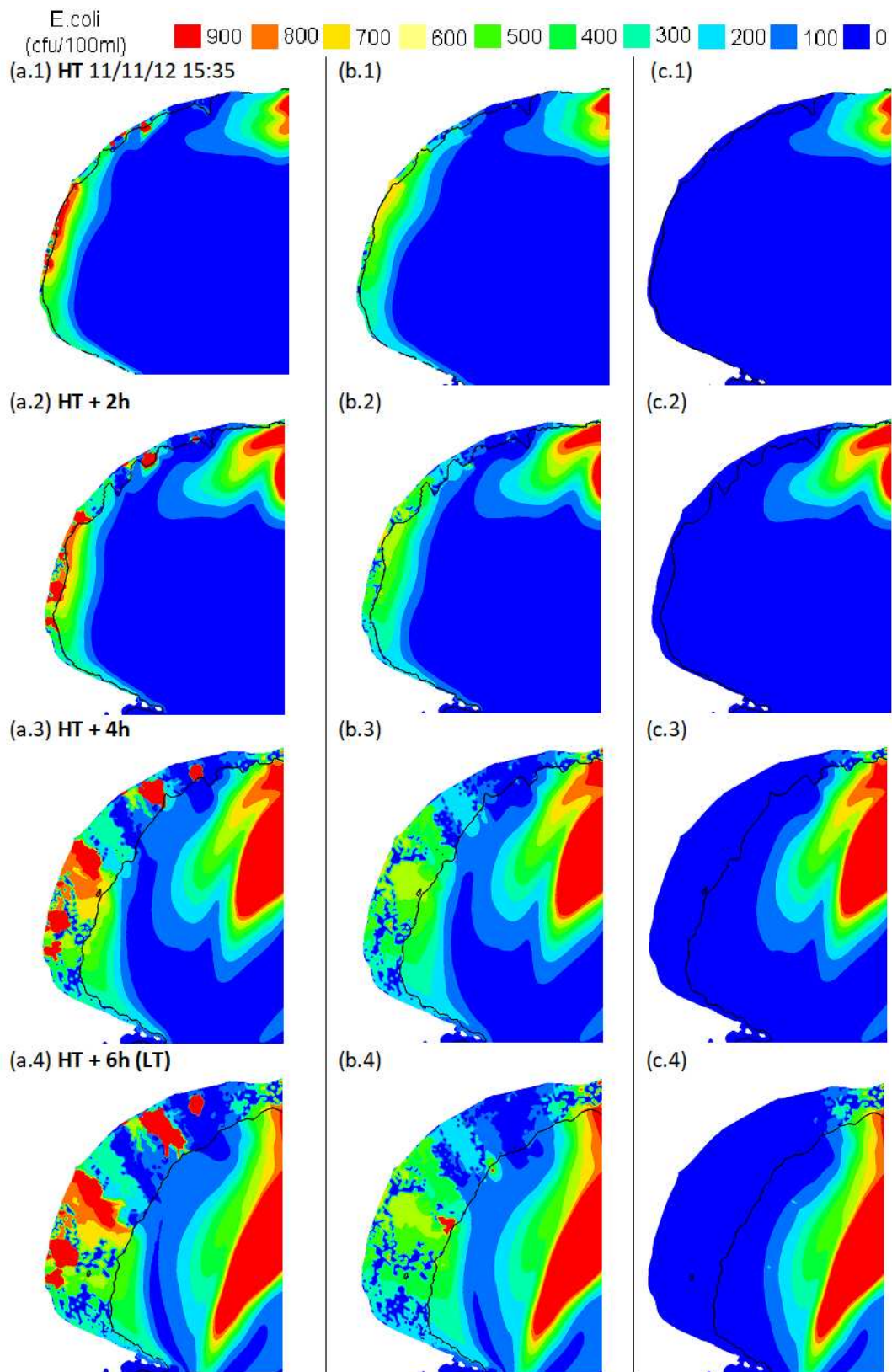
Figure 25: Comparison of the predicted E. coli concentration distributions in Swansea Bay, using the 2D model with static sources, improved source representation (TH = 0.05), and deep water sources; (a), (b) and (c), respectively

464

5   Discussion

5.1   Comparison of 2D and 3D decay model setup

It can be seen in Figure 20 that the 2D model predicts higher bacterial concentrations than the 3D

model. This can be partly attributed to the method used in inclusion of the rivers Tawe and Neath

in the 2D model, which were included in the 3D model by accumulating the flow and bacterial input

at a single point due to computational time issues, and can be explained by looking at Figures 26

and 27.
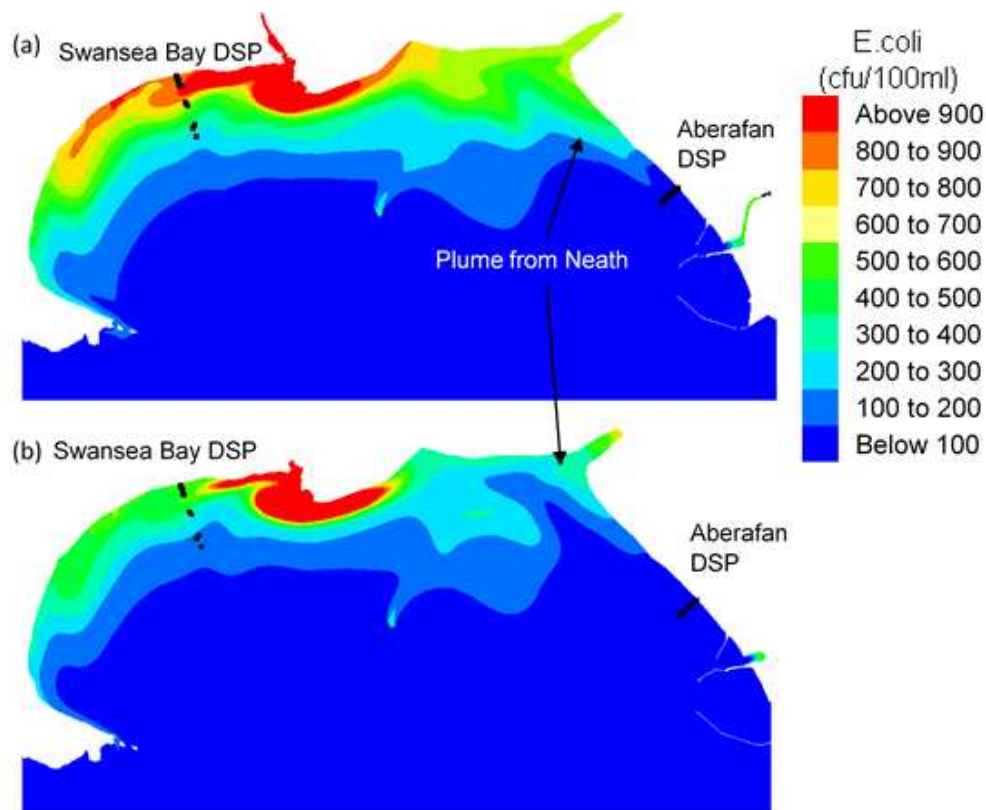
Figure 26: Comparison of the predicted E. coli concentration distribution in Swansea Bay, at 19:16

on 15/11/12 (HT), using the Stapleton et al. (2007a) decay function in the 2D (a) and 3D (b)

models. Depth-averaged decay function used in the 3D model
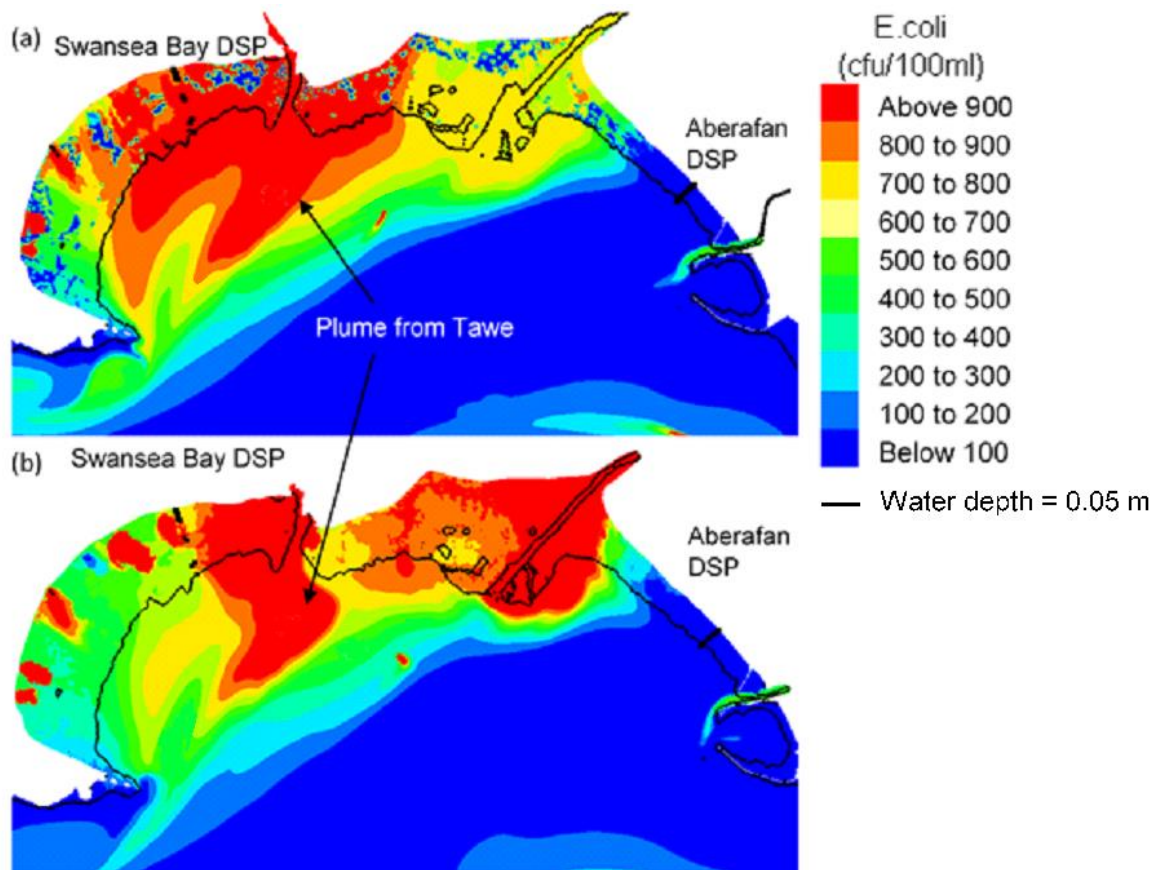
Figure 27: Comparison of the predicted E. coli concentration distribution in Swansea Bay, at 12:09 on 15/11/12 (LT), using the Stapleton et al. (2007a) decay function in the 2D (a) and 3D (b) models. Depth-averaged decay function used in the 3D model. The black line represents a water depth of 0.05 m.

Based on the location of the model *E. coli* inputs (see Figures 4 and 5), it can be reasoned that the plume from the River Tawe is responsible for the water quality at the Swansea Bay DSP. While this input is included accurately within the 2D model, it is represented as a point source at the river mouth in the 3D model, without an assigned velocity. In this case the flow speed is greatly reduced and the plume does not extend far enough into the Bay during the ebb tide. This highlights the importance of including source term momentum when representing bacterial inputs in 3D models. This may be either by assigning a velocity to point sources or linking 1D river models with the 3D coastal model, with momentum transfer across the linked boundaries.

5.2   Spatial and temporal variability

It is suggested that because of the spatial variance in bacterial concentrations shown in Figures 21 and 22, when modelling and sampling it may be prudent to predicted and record FIO levels at multiple locations to ascertain the spatial distribution in bacterial concentration and adequately determinate the risk to bathers. Not doing so may lead to under prediction of this risk and erroneous calibration of the hydro-epidemiological models.

In addition, Figure 21 shows a diurnal pattern in the predicted *E. coli* concentrations at the Swansea Bay DSP. On day 320 this is also seen in the measured data. This diurnal pattern is expected to be due to the accumulative impact of decay during the day following an increase in the solar radiation, as shown in Figure 15. However, other influential factors might be affecting the diurnal pattern, such as a contribution from the sources, tidal dilution or interaction with sediments, and which need to be considered in more detail.

High spatial, and potentially diurnal, variations are seen along all other transects too, thus highlighting the variability of the concentration along a beach and at different times. Therefore, although this highlights a potential limitation of the model to calculate processes which take place at a high spatial resolution, it may also be prudent to consider different methods of classifying bathing water sites based on a non-stationary DSP.

5.3   Depth-varying decay

It can be seen in Figure 23 that lower concentrations were predicted when using the depth-varying decay function. To discuss the reason for this reduction in concentration and highlight the applicability of the depth-averaged decay approach, a simplified vertical 1D case is considered. Equation 15 represents a simplified form of Equation 1, reduced to 1D in the vertical and with zero vertical velocity.

$$\frac{\partial C}{\partial t} = \frac{\partial}{\partial z}\left(v_T \frac{\partial C}{\partial z}\right) - kC \qquad\qquad 15$$

516

517   In this situation the problem is reduced to one controlled by turbulent and molecular diffusion

518   between the layers and decay. This can be further reduced to Equation 2 by setting the turbulent

519   diffusion term to zero. The analytical solution of Equation 15 is then given in Equation 16:

520

$$C(t) = C_0 e^{-kt} \qquad\qquad 16$$

521

522   where C(t) is the concentration at time t, C_0 is the concentration at time t = 0 and k is the decay

523   rate (1/d). For a simple 5-layer problem, with a node spacing of 1 m, we look at the decay of an

524   initial tracer (bacteria) concentration of 1,000 (dimensionless) over 2 days. The equation was

525   solved at a time step of 1 minute using the finite different method, with a first order forward

526   difference scheme in time and a second order central difference scheme in space. The boundary

527   value problem was solved at the surface and bed introducing phantom layers, with a value equal

528   to the adjacent real boundary. Thus, diffusion only acts within the domain. Values for suspended

529   sediment concentration, salinity and temperature were set as those used in the Swansea Bay

530   study, and with the light intensity fixed at 260 W/m^2.

531

532   A comparison of the concentrations over depth predicted by the analytical solution and two

533   different decay approaches used in this study is illustrated in Figure 28. As can be seen there is

534   good agreement between the analytical solution and the finite difference solutions, using a depth-

535   varying decay, when the tracer diffusion term is set to zero. This result confirms the validity of this

536   method. For further information, see King (2019) wherein the data plotted in (a) is presented in

537   tabular form. Comparing the use of the depth-varying and depth-averaged decay functions, it can

538   be seen in (b) that the overall concentration in the water column is less when a depth-varying

539   approach was used. This is because the exponentially larger decay rate in the surface layers causes

540   a greater reduction in the concentration than that predicted at depth (see Figure 7).

541

542   Due to the increased transport of bacteria from regions of high concentration at depth to lower

543   concentrations at the surface, this results in higher concentrations in the surface layers, reduced

544   concentrations at depth and a reduction in total concentration in the water column. Bacteria in the

545   surface layers continues to decay at a faster rate, increasing the concentration gradient and hence

546   the movement of bacteria between layers.
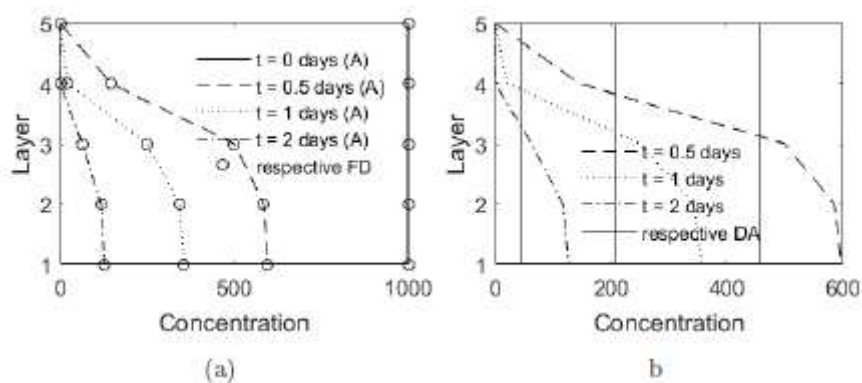
547

548   *Figure 28: Solution of simplified 5 layer decay problem; (a) comparison between analytical and*

549   *finite difference (FD) solutions using a depth-varying decay rate, where T = 0; and (b)*

550   *comparison between FD solutions using depth-averaged (DA) and varying solutions*

551   This interchange between layers will be further increased by including the velocity term in

552   Equation 15, where there is an upward flow such as in Swansea Bay, and in the vicinity of long

553   sea outfall diffusers with a vertical orientation.

5.4   Moving discharge

555   The following section presents a comparison between the use of static and non-stationary

556   bacterial point inputs in the 2D model of Swansea Bay. In considering the predicted surface

557   concentration distributions (see Figure 25), there are clear differences observed when comparing

558   the two approaches over a tidal cycle. At high tide there are elevated concentrations in the static

559   discharge model and the *E. coli* plume extends a greater distance into the western region of

560   Swansea Bay. During the ebb tide the differences become more pronounced as the plume spreads

561   over a larger beach area above the water line. In comparison, the predicted concentrations in the

562   improved source model are greatly reduced and the plume below the water line is reduced in size.

563   There are also small regions with high *E. coli* concentrations immediately below the waterline, and

564   in the vicinity of the source points, which have more serious implications on the predicted risk to

565   bathers. Therefore, implementation of the mobile source point could significantly impact the

566   results and should be considered in future studies. With regard to the *E. coli* distribution above the

567   water line, this will have a greater implication if the beach sand is considered as a diffuse bacterial

568   source and sink, in a similar manner to how Abu Bakar et al. (2017b) modelled inter-tidal

569   marshland in the Loughor Estuary, UK. Furthermore, these regions may aid in providing more

570   accurate predictions of the location of 'safe' and 'no go zones', on the beach and in the water, which

571   is of utmost importance when disseminating bathing water information to beach goers, as advised

572   in the rBWD.

573   As shown in Figure 24, for the majority of the simulation period, use of the improved source model

574   results in lower concentrations. This is due to increased dilution as the tracer is released into

575   deeper water. While it is not possible to discern a difference between the two improved source

576   models using different threshold depths, it can be seen in Figure 25 that if all release locations are

577   moved to a point below the low tide line, *E. coli* concentrations in the nearshore region are under

578   predicted throughout the tidal cycle, due to increased dilution. This indicates that correctly

579   modelling the beach sources is important in order to predict accurately the dynamics governing

580   bacterial transport. It is therefore suggested that the apparent invariance between the static and

581   improved source release models seen in Figure 24 is due to the distance of the DSP from the

582   bacterial beach source locations (see Figure 1), as well as the influence of the River Tawe on the

583   DSP as previously explained.

584   It can be seen from these results that although using the new model results in minor

585   improvements in *E. coli* concentration predictions at the DSP and within Swansea Bay, the

586   differences between model predictions are not significant enough to warrant the choice of one

587   method over the other for this case study, or at this stage in model development.

588

6   Conclusions

590   Two computational models, one 2D and one 3D, were set up using the TELEMAC suite of models

591   to implement new enhancements in simulating the transport and decay of *E. coli* in a data rich case

592   study site. The models and the data were then compared for a range of different modelling

593   approaches. The case study site was Swansea Bay, located in South West of the UK, where over

594   7,000 samples were taken during 2011. The 3D model was found to under predict bacterial

595   concentrations due to the inclusion of the Rivers Neath and Tawe as point sources, and without

596   momentum conservation. The application of a 3D model in a well-mixed marine environment,

597   where a 2D depth averaged approach is usually adopted, highlights the impact of a vertically

598   variable decay through the water column. Application of this method is an important step in

599   improving the reliability of 3D deterministic epidemiological models, to ensure that decay

600   processes are represented realistically. Of the two methods used to calculate decay throughout the

601   water column in the 3D model, namely depth-varying and depth-averaged, the depth-varying

602   approach was found to predict lower bacterial concentrations due to the exponential decrease in

603   light intensity with depth and the associated effect on the decay rate. It is therefore suggested that

604   in 3D modelling studies a depth-varying decay model should be used as it provides a more

605   accurate representation of the vertical spatial variation in bacterial die-off rates. Using the 2D

606   model, an improved method of representing beach sources was developed to mimic the streams

607   discharging along the Swansea Bay beach. Rather than being considered stationary, the sources

608   were moved along a transect throughout the simulation period, to ensure they discharged just

609   below the waterline. This provided more accurate predictions of the spatial distribution of *E. coli*

610   within the domain, with the most significant effects noticed above and near the waterline, such as

611   zones of elevated bacterial concentration where the beach streams enter the water. In addition, it

612   highlights the limitations of using TELEMAC to model static beach sources on shallow gradient

beaches, subject to wetting and drying throughout the tidal cycle. Spatial and diurnal variations in

bacterial concentrations were seen along the Swansea Bay Designated Sampling Point transect,

highlighting the variability of water quality along the beach and at different times. Therefore, it is

suggested that bathing water monitoring based on a stationary Designated Sampling Point may

lead to incorrect classification of the bathing water quality and provide a false indication of the

risk of infection. In addition, it highlights a potential limitation of bacterial models to calculate

processes accurately, which take place at a high spatial resolution.

Acknowledgements

References

Aberystwyth University and University College Dublin, 2018. Smart Coasts [online]. Available from: http://smartcoasts.eu/ [accessed 18 August 2018].

Abu Bakar, A., Ahmadian, R. and Falconer. R.A., 2017a. Modelling the transport and decay processes of microbial tracers released in a macro-tidal estuary. Water Research. 123, October, 802-824.

637   Abu Bakar, A., Ahmadian, R. and Falconer. R.A., 2017b. Diffuse bacteria loading from intertidal
638   marshland and impacts to adjacent estuarine water quality. Proceedings of the 37th IAHR
639   World Congress, pp. 3563-3570.

640   Ahmadian, R., Falconer, R. A. and Lin, B., 2010. Hydro-environmental modeling of the proposed
641   Severn barrage. Proceedings of the Institution of Civil Engineers Energy 163(3), pp. 107-117.
642   https://doi.org/10.1680/ener.2010.163.3.107.

643   Ahmadian, R., Bomminayuni, S., Falconer. R.A. and Stoesser, T., 2013. SSC Numerical modelling of
644   flow and faecal indicator organism transport at Swansea Bay, UK. Technical Report.

645   Ahmadian, R., Olbert, A.I., Hartnett, M. and Falconer, R.A., 2014. Sea level rise in the Severn Estuary
646   and Bristol Channel and impacts of a Severn Barrage. Computers & Geosciences, 66, pp. 94-105.

647   Alkan, U., Elliott, D. J. and Evison, L. M. 1995. Survival of enteric bacteria in relation to simulated
648   solar radiation and other environmental factors in marine waters. Water Research, 29(9), pp.
649   2071-2080. https://doi.org/10.1016/0043-1354(95)00021-C.

650   BBC, 2017. UK attracting record numbers of tourists [online]. Available from:
651   https://www.bbc.co.uk/news/business-41564655 [accessed 3 December 2018].

652   Bedri, Z., Bruen, M., Dowley, A. and Masterson, B., 2013. Environmental consequences of a power
653   plant shutdown: A three-dimensional water quality model of Dublin Bay. Marine Pollution
654   Bulletin, 71(1-2), pp. 117–128. https://doi.org/10.1016/j.marpolbul.2013.03.025.

655   Bedri, Z., Corkery, A., O'Sullivan, J. J., Alvarez, M. X., Erichsen, A. C., Deering, L. A., Demeter, K.,
656   O'Hare, G. M. P., Meijer, W. G. and Masterson, B., 2014. An integrated catchment-coastal
657   modelling system for real-time water quality forecasts. Environmental Modelling and Software,
658   61, pp. 458–476. http://dx.doi.org/10.1016/j.envsoft.2014. 02.006.

659   Bedri, Z., O'Sullivan, J. J., Deering, L. A., Demeter, K., Masterson, B., Meijer, W. G., and Hare. G. O.,
660   2015. Assessing the water quality response to an alternative sewage disposal strategy at

661   bathing sites on the east coast of Ireland. Marine Pollution Bulletin, 91(1), pp. 330–346.

662   http://dx.doi.org/10.1016/j.marpolbul.2014.11.008.

663   Bedri, Z., Corkery, A., O'Sullivan, J. J., Deering, L. A., Demeter, K., Meijer, W. G., Masterson, B., 2016.

664   Evaluating a microbial water quality prediction model for beach management under the

665   revised EU Bathing Water Directive. Journal of Environmental Management, 167, pp. 49–58.

666   https://doi.org/10.1016/j.jenvman.2015.10.046.

667   Bomminayuni. S., 2015. Modelling tidal ow for assessment of hydro-kinetic energy and bathing

668   water quality in coastal waters. PhD thesis.

669   Boye, B. A., Falconer. R.A., and Akande. K., 2015. Integrated water quality modelling: Application

670   to the Ribble Basin, U.K. Journal of Hydro-environment Research, 9(2), pp. 187-199.

671   https://doi.org/10.1016/ j.jher.2014.07.002.

672   Chapra. S. C., 1997. Surface Water-Quality Modeling. Mc-Graw Hill, Singapore.

673   Bussi, G., Whitehead, P. G., Thomas, A. R.C., Masante, D., Jones, L., Cosby, J.B., Emmett, B. A., Malham,

674   S. K., Prudhomme, C., Prosser, H., 2017. Climate and land-use change impact on faecal indicator

675   bacteria in a temperate maritime catchment (the River Conwy, Wales). Journal of Hydrology.

676   https://doi.org/10.1016/j.jhydrol.2017.08.011.

677   Chen, W. B. and Liu, W. C., 2017. Investigating the fate and transport of fecal coliform

678   contamination in a tidal estuarine system using a three-dimensional model. Marine Pollution

679   Bulletin, 116(1-2), pp. 365–384. https://doi.org/10.1016/j.marpolbul.2017.01.031.

680   Chow, V. T. 1959. Open-channel hydraulics. McGraw-Hill Book Company, New York.

681   Což, N., Ahmadian, R., Falconer, R.A., 2019. Implementation of a full momentum conservative

682   approach in modelling flow through tidal structures. Water, 11(9), 1917.

683   https://doi.org/10.3390/w11091917.

684   de Brauwere, A., de Brye, B., Servais, P., Passerat, J. Deleersnijder, and E., 2011. Modelling

685   Escherichia coli concentrations in the tidal Scheldt river and estuary. Water Research, 45(9),

686   pp. 2724–2738. https://doi.org/10.1016/j.watres.2011.02.003.

687   DHI, 2017a. Bathing Water Quality Forecast at Your Fingertips [online]. Available from:

688   https://www.   dhigroup.com/global/news/2017a/02/bathing-water-quality-forecast-at-

689   your-fingertips.

690   DHI, 2017b. Water Forecast [online]. Available from: http://www.waterforecast.com/.

691   Droste, R. L., 1997. Theory and Practice of Water and Wastewater Treatment. John Wiley & Sons,

692   Inc, New York.

693   EMU Limited, 2012. Swansea Bay Current Monitoring Operational Report. Technical report.

694   European Environment Agency, 2005. Bathing Water Quality [online]. Technical report. Available

695   at: http://www.eea.europa.eu/data-and-maps/indicators/bathing-water-quality [accessed 27

696   January 2016].

697   European Parliament, 2006. Directive 2006/7/EC of the European Parliament and of the Council

698   of 15 February 2006 concerning the management of bathing water quality and repealing

699   Directive 76/160/EEC. Official Journal of the European Union, L 064/37.

700   Feng, Z., Reniers, A., Haus, B. K., Solo-Gabriele, H. M., Wang, J. D., and Fleming, L. E., 2015. A

701   predictive model for microbial counts on beaches where intertidal sand is the primary source.

702   Marine Pollution Bulletin, 94(1-2), pp. 37–47. https://doi.org/10.1016/j.marpolbul.2015.03.019.

703   DeFlorio-Barker, S., Wing, C., Jones, R. M. and Dorevitch. S., 2018. Estimate of incidence and cost of

704   recreational waterborne illness on United States surface waters. Environmental Health: A

705   Global Access Science Source, 17(1):3. https://doi.org/10.1186/s12940-017-0347-9.

706   Given,, S., Pendleton, L. H., and Boehm, A. B., 2006. Regional public health cost estimates of

707   contaminated coastal waters: A case study of gastroenteritis at southern California beaches.

708   Environmental Science and Technology, 40(16), pp. 4851-4858.

709   https://doi.org/10.1021/es060679s.

710   Galland, J. C., Goutal, N., and Hervouet. J. M., 1991. TELEMAC: A new numerical model for solving

711   shallow water equations. Advances in Water Resources, 14 (3), pp. 138-148.

712   https://doi.org/10.1016/0309-1708(91)90006-A.

713   Guo, B., Ahmadian, R., Evans, P., Falconer, R.A. (2020). "Studying the Wake of an Island in a

714   Macro-Tidal Estuary." Water (2020) 12, 1225.

715   J. F. Guillaud, A. Derrien, M. Gourmelon, and M. Pommepuy. T90 as a tool for engineers: Interest

716   and limits. Water Sciences and Technology, 35(11-12):277–281, 1997.

717   Lea, W., 1996. Bathing water quality. Science and Environment Section. House of Commons

718   Library, 96/45.

719   J.-M. Hervouet. Hydrodynamics of Free Surface Flows: Modelling with the Finite Element Method.

720   Wiley, Chichester, 2007. URL http://eu.wiley.com/WileyCDA/WileyTitle/productCd-

721   0470035587.html.

722   Huang, G., Falconer, R. A. and Lin, B. 2015. Integrated river and Coastal flow, sediment and

723   Escherichia coli modelling for bathing water quality. Water 7(9), pp. 4752-4777.

724   (10.3390/w7094752)

725   Huang, G., Falconer. R.A. and Lin, B., 2018. Evaluation of E.coli losses in a tidal river network

726   using a refined 1-D numerical model. Environmental Modelling & Software.

727   https://doi.org/10.1016/j.envsoft.2018.07.009.

728   Iman, R. L., 2008. Latin Hypercube Sampling. Encyclopedia of Quantitative Risk Analysis and

729   Assessment. John Wiley & Sons, Ltd. https://doi.org/10.1002/9780470061596.risk0299.

730   King, J., 2019. Investigation and prediction of pollution in coastal and estuarine waters, using

731   experimental and numerical methods. PhD Thesis, Cardiff University, Cardiff.

732 Kopmann, R. and Markofsky, M., 2000. Three-dimensional water quality modelling with

733 TELEMAC-3D. Hydrological Processes, 14(13), pp. 2279–2292,

734 https://doi.org/10.1002/1099-1085(200009)14:13h2279:: AID-HYP28i3.0.CO;2-7.

735 Mancini, J. L., 1978. Numerical Estimates of Coliform Mortality Rates under Various Conditions.

736 Water Pollution Control Federation, 50(11), pp. 2477–2484.

737 Mattioli, M. C., Sassoubre, L. M., Russell, T. L, and Boehm, A. B., 2017. Decay of sewage-sourced

738 microbial source tracking markers and fecal indicator bacteria in marine waters. Water

739 Research, 108, pp. 106– 114. https://doi.org/10.1016/j. watres.2016.10.066.

740 Nash J. E. and Sutcliffe, J. V., 1970. River Flow Forecasting Through Conceptual Models Part I-a

741 Discussion of Principles. J. Hydrology, 10(3), pp. 282–290. https://doi.org/10.1016/0022-

742 1694(70)90255-6.

743 Scottish Government, 2018. Value of bathing waters and influence of bathing water quality:

744 Technical research report. Technical report. https://www.gov.scot/publications/. Accessed:

745 2018-12-03.

746 Stapleton, C. M., Wyer, M. D., Kay, D., Bradford, M., Humphrey, N., Wilkinson, J., Lin, B., Yang, L.,

747 Falconer. R.A. , Watkins, J., Francis, C. A., Crowther, J., Paul, N. D., Jones, K., and McDonald, A. T.,

748 2007a. Fate and transport of particles in estuaries - Volume IV: Numerical modelling for

749 bathing water enterococci estimation in the Severn estuary. Technical report, Environment

750 Agency, Bristol. Technical report.

751 Stapleton, C. M., Wyer, M. D., Kay, D., Bradford, M., Humphrey, N., Wilkinson, J., Lin, B., Yang, L.,

752 Falconer. R.A. , Watkins, J., Francis, C. A., Crowther, J., Paul, N. D., Jones, K., and McDonald, A. T.,

753 2007b. Fate and transport of particles in estuaries - Volume III : Laboratory experiments ,

754 enterococci decay rates and association with sediments. Environment Agency, Bristol.

755 Technical report.

756 Stein, M., 1987. Large Sample Properties of Simulations Using Latin Hypercube Sampling.

757 Technometrics, 29(2), pp.143-151.

758 The University of Edinburgh, 2016a. EDINA Marine Digimap Service [online]. Available from:

759 https://digimap.edina.ac.uk/ [accessed: 1 September 2016].

760 The University of Edinburgh, 2016b. 1 Arcsecond Gridded Bathymetry (ASC geospatial data)

761 [online]. Available from: http://digimap.edina.ac.uk [accessed 1 September 2016].

762 Thomann, R. V., and Mueller, J. A., 1987. Principles of Surface Water Quality Modeling and Control.

763 HarperCollins, New York.

764 Visit Britain, 2017. GB Tourism Survey: 2017 overview [online]. Available from:

765 https://www.visitbritain.org/gb-tourism-survey-2017-overview [accessed 3 December

766 2018].

767 Weiskerger, C. J. and Phanikumar, M. S., 2020. Numerical Modeling of Microbial Fate and Transport

768 in Natural Waters: Review and Implications for Normal and Extreme Storm Events. Water,

769 12(7), 1876.

770 White, E., Saunders, A., Gibson, J., and Barcock, N., 2014. Tidal Lagoon Swansea Bay Marine Water

771 Quality Assessment. Supporting Technical Information. Tidal Lagoon Swansea Bay Limited.

772 Technical report.

773 World Health Organization, 2003. Guidelines for safe recreational water environments. Volume 1,

774 Coastal and fresh waters. World Health Organization.

775 https://apps.who.int/iris/handle/10665/42591.

776 Xu, P., Brissaud, F., and Fazio, A., 2002. Non-steady-state modelling of faecal coliform removal in

777 deep tertiary lagoons. Water Research, 36(12), pp. 3074–3082.

778 https://doi.org/10.1016/S0043-1354(01) 00534-6.

779 Yang, L., Lin, B. and Falconer, R. A, 2008. Modelling enteric bacteria level in coastal and estuarine

780 waters. Proceedings of the Institution of Civil Engineers Engineering and Computational

781 Mechanics 161(4), pp. 179-186.